# Numerical calculation method for the scouring phenomenon

**Syaoyue Chen,[1] Kohei Suzuki,[2] Taro Arikawa[3] and Masashi Watanabe[4]**

[1]Coastal Engineering Laboratory, Civil and Environmental Engineering, Chuo University, 1-13-27 Kasuga, Bunkyo-ku, Tokyo 112-8551, Japan; email: a15.wsrd@g.chuo-u.ac.jp
[2]CTI Engineering Co., Ltd., 2-4-12 Daimyou, Chuo-ku, Fukuoka 810-0041, Japan; email: kh-suzuki@ctie.co.jp
[3]Corresponding Author, Coastal Engineering Laboratory, Civil and Environmental Engineering, Chuo University, 1-13-27 Kasuga, Bunkyo-ku, Tokyo 112-8551, Japan; email: taro.arikawa.38d@g.chuo-u.ac.jp
[4]Coastal Engineering Laboratory, Civil and Environmental Engineering, Chuo University, 1-13-27 Kasuga, Bunkyo-ku, Tokyo 112-8551, Japan; email: watanabe.07w@g.chuo-u.ac.jp

## ABSTRACT

This study used CADMAS-SURF / 3D to calculate and explore the scouring phenomenon of past experiments and to compare the results between the calculation and the experiments to examine the validity of this method.

As the result of verifying the response in the ground, it is possible to simulate the pore water pressure inside the ground using this method. Moreover, the maximum scour depth and location are similar to those of the experimental values. Thus, the accuracy of this numerical model was proved in this study.

## INTRODUCTION

In the 2011 Great East Japan Earthquake, tsunamis that overflowed breakwaters and seawalls scoured behind the seawalls. As a result, the dam bodies lost their ground support capacity and fell. Previously, protection policy did not allow inundation behind breakwaters and seawalls, but after the earthquake, when designing protection facilities, the possibility of a tsunami crossing a dike was considered. It was designed to have a structure that is tenacious even if it allows overflow, and therefore exhibits a protective effect. To realize such a structure, it was necessary to consider the influence of scouring behind breakwaters or seawalls at the time of overflow. However, there is little knowledge about the amount of scouring due to overflow, and there are many unclear parts about the relationship between overflow and drop height.

Previous experimental study by Arikawa et al.(2014) showing settlement of a breakwater intended to block and dissipate waves showed that scaling of sand particle movement is difficult in small-scale experiments. It is important to allow the particle-size ratio between the mounds of stone and the sand to be the same as the real scale ratio. However, it remains difficult to elucidate phenomena using experimental studies.

In this study, CADMAS-SURF / 3D was used to reproduce the scouring phenomenon of past experiments and the calculated and experimental results were compared to examine the validity of this method.

## NUMERICAL MODEL

### CADMAS-SURF/3D

**Basic equation** As the basic equations of CADMAS-SURF / 3D, equations (1–4) were obtained by extending the continuous equation for three-dimensional (3-D) incompressible viscous fluids and the Navier-Stokes equations, were adopted based on a porous model.

- Continuous equation

$$\frac{\partial \gamma_x u}{\partial x} + \frac{\partial \gamma_y v}{\partial y} + \frac{\partial \gamma_z w}{\partial z} = \gamma_v S_\rho \tag{1}$$

- Navier-Stokes equations

$$\lambda_v \frac{\partial u}{\partial t} + \frac{\partial \lambda_x uu}{\partial x} + \frac{\partial \lambda_y vu}{\partial y} + \frac{\partial \lambda_z wu}{\partial z} = -\frac{\gamma_v}{\rho}\frac{\partial p}{\partial x} + \frac{\partial}{\partial x}\left\{\gamma_x v_e \left(2\frac{\partial u}{\partial x}\right)\right\} + \frac{\partial}{\partial y}\left\{\gamma_y v_e \left(\frac{\partial u}{\partial y} + \frac{\partial v}{\partial x}\right)\right\} + \frac{\partial}{\partial z}\left\{\gamma_z v_e \left(\frac{\partial u}{\partial z} + \frac{\partial w}{\partial x}\right)\right\} - \gamma_v D_x u - R_x + \gamma_v S_u \tag{2}$$

$$\lambda_v \frac{\partial v}{\partial t} + \frac{\partial \lambda_x uv}{\partial x} + \frac{\partial \lambda_y vv}{\partial y} + \frac{\partial \lambda_z wv}{\partial z} = -\frac{\gamma_v}{\rho}\frac{\partial p}{\partial y} + \frac{\partial}{\partial x}\left\{\gamma_x v_e \left(\frac{\partial v}{\partial x} + \frac{\partial u}{\partial y}\right)\right\} + \frac{\partial}{\partial y}\left\{\gamma_y v_e \left(2\frac{\partial v}{\partial y}\right)\right\} + \frac{\partial}{\partial z}\left\{\gamma_z v_e \left(\frac{\partial v}{\partial z} + \frac{\partial w}{\partial y}\right)\right\} - \gamma_v D_y v - R_y + \gamma_v S_v \tag{3}$$

$$\lambda_v \frac{\partial w}{\partial t} + \frac{\partial \lambda_x uw}{\partial x} + \frac{\partial \lambda_y vw}{\partial y} + \frac{\partial \lambda_z ww}{\partial z} = -\frac{\gamma_v}{\rho}\frac{\partial p}{\partial z} + \frac{\partial}{\partial x}\left\{\gamma_x v_e \left(\frac{\partial w}{\partial x} + \frac{\partial u}{\partial z}\right)\right\} + \frac{\partial}{\partial y}\left\{\gamma_y v_e \left(\frac{\partial w}{\partial y} + \frac{\partial v}{\partial z}\right)\right\} + \frac{\partial}{\partial z}\left\{\gamma_z v_e \left(2\frac{\partial w}{\partial z}\right)\right\} - \gamma_v D_z w - R_z + \gamma_v S_w + \frac{\gamma_v \rho^* g}{\rho} \tag{4}$$

In the equation above, $t$ is time; $x, y$ is horizontal coordinate; $z$ is the vertical coordinate; and $u, v, w$ are flow velocity components in the $x, y, z$ directions. Here, $\rho$ is the reference density; $\rho^*$ is the density considering buoyancy; and $p$ is pressure. The term $v_e$ is the sum of the molecular kinematic viscosity coefficient $v$ and eddy viscosity coefficient $v_t$; while $g$ is gravitational acceleration. Here, $\gamma_v$ is porosity; $\gamma_x, \gamma_y, \gamma_z$ are area transmittances in $x, y, z$ directions; and $D_x, D_y, D_z$ are coefficients for the energy decay zone. The source terms $S_\rho, S_u, S_v, S_w$ are for wave-making sources and the terms $\lambda_v, \lambda_x, \lambda_y, \lambda_z$ are shown in equation (5). Here, $C_M$ is the inertia force coefficient in (5). The second term is the effect of the inertial force received from the structure.

$$\begin{cases} \lambda_v = \gamma_v + (1-\gamma_v)C_M \\ \lambda_x = \gamma_x + (1-\gamma_x)C_M \\ \lambda_y = \gamma_y + (1-\gamma_y)C_M \\ \lambda_z = \gamma_z + (1-\gamma_z)C_M \end{cases} \tag{5}$$

The resistances $R_x, R_y, R_z$ from the porous body are modeled in proportion to the square of the flow velocity, as shown in equation (6), using $C_D$ as the resistance coefficient.

$$\begin{cases} R_x = \frac{1}{2}\frac{C_D}{\Delta x}(1-\gamma_x)u\sqrt{u^2+v^2+w^2} \\ R_y = \frac{1}{2}\frac{C_D}{\Delta y}(1-\gamma_y)v\sqrt{u^2+v^2+w^2} \\ R_z = \frac{1}{2}\frac{C_D}{\Delta z}(1-\gamma_z)w\sqrt{u^2+v^2+w^2} \end{cases} \quad (6)$$

The terms $\Delta x, \Delta y, \Delta z$ are the grid size in $x, y, z$ directions.

**Discretization policy** Numerical simulation using CADMAS-SURF/3D was performed based on the SMAC (Simplified Marker and Cell) algorithm. The discretization policy is as follows.

- A staggered grid system is used.
- A variable grid width which is able to set the grid width freely is used.
- The basic equations described in the storage format are discretized using the control volume method.
- The difference in the spatial direction other than the advection term is the central difference of secondary accuracy, and the difference other than the advection term is the windward difference.
- The interpolation method uses linear interpolation and area interpolation.
- The discretization in the time direction is based on the Euler method, and the SMAC method (which implicitly evaluates the pressure term) is used for coupling the equation of motion and the continuity equation.

**Free surface treatment method** The free surface analysis model uses the VOF method, which is highly versatile and can analyze complex surface shapes. The VOF method analyzes the behavior of the free surface using an advection equation of the VOF function F, which averages the function representing "whether or not a fluid" for each calculation cell, and calculates the surface orientation sequentially. Equation (7) shows the advection equation of the VOF function F based on the porous model.

$$\gamma_v \frac{\partial F}{\partial t} + \frac{\partial \gamma_x u F}{\partial x} + \frac{\partial \gamma_y v F}{\partial y} + \frac{\partial \gamma_z w F}{\partial z} = \gamma_v S_F \quad (7)$$

Here, $S_F$ is the source term for making waves in equation (7).

**STM**

The model proposed by Takahashi et al. (1999) considers sediment transport by tsunami separately as a bed-load layer and a suspended-sand layer. The bed load layer includes modes of moving while maintaining contact with the bottom surface by sliding or rolling, as well as the mode called saltation (repeatedly popped up into the water column briefly and quickly returning to the bottom downstream). The suspended layer means that the vertical component of the turbulent stress is more powerful than the gravity acting on the sand grains, the sand grains are held up in the water column, and move within the flowing water. In addition, the handling of fluid motion is important in considering the sediment transport phenomenon in the suspended sand layer.

Therefore, in the Takahashi model, because a tsunami is involved, and the flow is evaluated using the discharge flux. Figure 1 shows a conceptual diagram of this model.

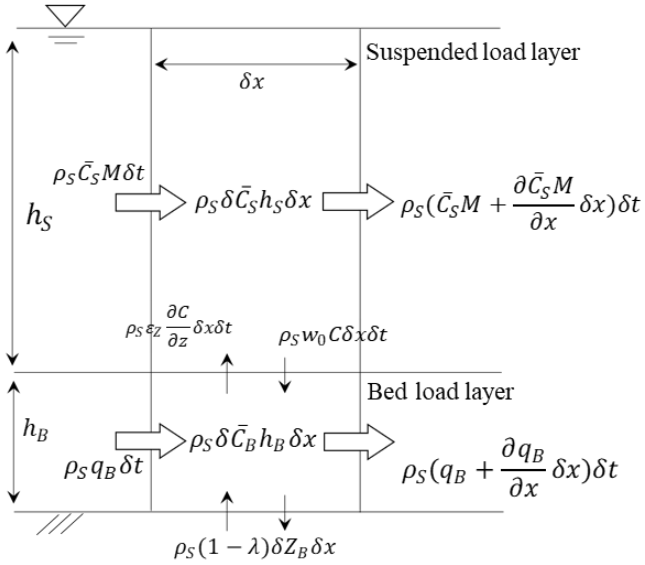


**Figure 1. Conceptual diagram of Takahashi's model**

Here, $\rho_s$ is the density of sand grains; λ is porosity of the sand grains; and $Z_B$ is the bottom height from the reference plane. The term $q_B$ is the bed load; while $\varepsilon_Z$ is the vertical diffusion coefficient; $C$ is the concentration near the boundary between bedload layer and suspended layer; and $w_0$ is the setting velocity of the sand grains. Here, $C_B$ is the average bed load concentration; $h_B$ is the thickness of the bedload sand layer; and $M$ is the flow flux.

Equation (8) shows the conventional continuous bed-sand formula.

$$\frac{\partial Z_B}{\partial t} + \frac{1}{1-\lambda} \frac{\partial q_B}{\partial x} = 0 \tag{8}$$

This model further considers the following things:

- Exchange sediment value with bottom (erosion and deposition).
- Balance of the amount of sediment transported in the downstream direction in the form of bed load.
- Sediment flux upward into the suspended sand layer driven by diffusion.
- Sediment flux downward from the suspended sand layer driven by gravity.
- The increase and decrease in the amount of sediment transport in the bed.

It can be expressed as follows:

$$\frac{\delta Z_B}{\delta t} + \frac{1}{1-\lambda} \left( \frac{\delta q_B}{\delta x} + \varepsilon_Z \frac{\delta C}{\delta Z} - w_0 C + \frac{\delta C_B h_B}{\delta t} \right) = 0 \tag{9}$$

Here, let $W_{ex}$ be the unit area, the amount of vertical sediment transported per unit time and show $W_{ex}$ as (10).

$$W_{ex} = \varepsilon_Z \frac{\delta C}{\delta z} - w_0 C \tag{10}$$

Therefore, Equation (9) can be rewritten as Equation (11).

$$\frac{\delta Z_B}{\delta t} + \frac{1}{1-\lambda}\left(\frac{\delta q_B}{\delta x} + W_{ex} + \frac{\delta C_B h_B}{\delta t}\right) = 0 \tag{11}$$

In this model, the temporal change in bed-load layer concentration is assumed to be sufficiently small compared to the other terms, so the fourth term in Equation (11) is omitted. Furthermore, considering the effect of bottom slope and expanding Equation (11) to two dimensions, the continuous equation of the bed-load layer in this model is expressed by the following formula.

$$\frac{\delta Z_B}{\delta t} + \frac{1}{1-\lambda}\left[\left\{\frac{\partial}{\partial x}\left(q_x - \varepsilon|q_x|\frac{\partial z}{\partial x}\right)\right\} - \left\{\frac{\partial}{\partial y}\left(q_y - \varepsilon|q_y|\frac{\partial z}{\partial y}\right)\right\} + w_{ex}\right] = 0 \tag{12}$$

Here, $\varepsilon$ is a coefficient from the formula by Watanabe et al. (1984).

Next, consider the conservation of mass in the suspended sand layer. The following are considered:

- Balance of the amount of sediment transported in suspended form in the downflow direction (suspended sand flux in shallow water flow)
- Sediment flux that is pushed up from the bed-load sand layer by diffusion.
- Sediment flux downward to the bed-load layer due to gravity.
- The increase and decrease in the amount of sediment transport in the suspended sand layer (appears as suspended sand concentration) is balanced.

By the above, the continuous equation of the suspended sand layer can be expressed by the following formula.

$$\frac{\partial(C_s h_s)}{\partial t} + \frac{\partial(MC_s)}{\partial x} + \frac{\partial(MC_s)}{\partial y} - w_{ex} = 0 \tag{13}$$

The term $C_S$ is the average suspended sand concentration; $h_s$ is the thickness of the suspended sand layer; and $M$ is flow flux; $w_{ex}$ is amount of exchanged sand that flows into suspended sand layer from bed load sand layer.

**Coupling calculation method**

In this study, CADMAS-STM was coupled as shown in Figure 2. First, the fluid was calculated on the CADMAS side. Then, the flow velocity and water level were given on the STM side, and the topographic change was returned to the CADMAS side for calculation. The friction velocity was calculated from the average flow speed from the Manning velocity first, and the Shields number was calculated using the calculated friction velocity. The amount of bed load and the amount of hoisting were calculated from the calculated the Shields number. Finally, the amount of ground change was calculated using the calculated values in the continuous equation of the bed and the suspended sand layers.

## CONTROL EXPERIMENT

The results from this study were compared with those of a large-scale experiment by Arikawa et al. (2014), which reproduced scouring behind an upright seawall due to overflow.

**Experimental conditions** In an experiment by Arikawa et al. (2014), a 1/10 scale model of the experimental waterway was installed (184 m in length and 3.5 m in width) (Figure 3). The upright seawall was a stack of 2.04 m-wide concrete blocks, and the sand behind it was medium sand with a median particle size of 0.043 cm.

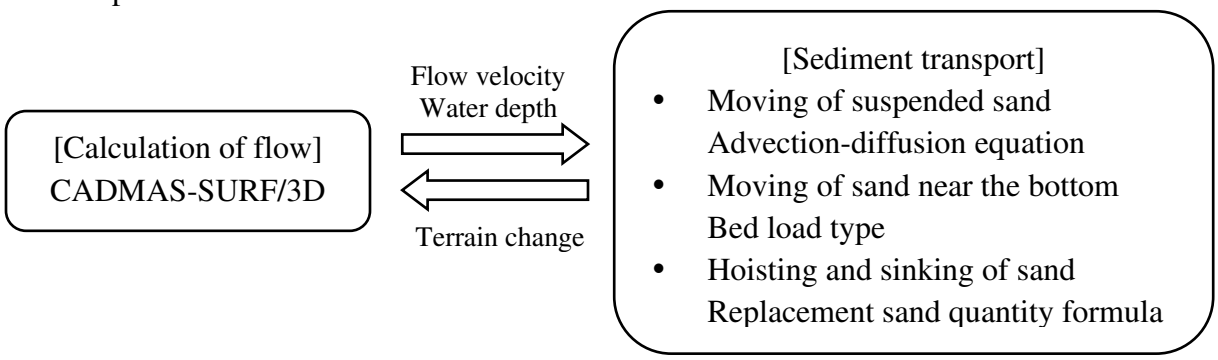


**Figure 2. Coupling calculation method.**

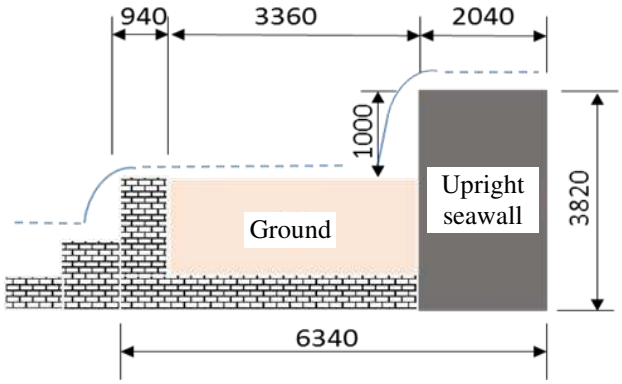


**Figure 3. Sectional view of the experimental model. (Unit: mm)**

The experiment caused flow by a reflux device in the experimental waterway. Scouring occurs due to a difference in the water level between the inflow side and the outflow side. The experiment was performed until the scour depth reached equilibrium. The original experimental conditions compared with those in this study, are shown in Table 1.

| | |
|---|---|
| Overflow drop height | 1.0m |
| Overflow flow rate | 0.29m$^2$/s |
| Median particle size of sand | 0.43mm |

**Table 1. Experimental conditions**

## CALCULATION

### Condition

The modeling in the numerical calculation (Figure 4) was the same as in the experiment, as shown in Figure 3. The overflow condition was reproduced by changing the initial water level.

The grid-cell size was set to 5 cm, and the depth was set to 25 cm in consideration of the calculation load. The water level difference $h$ was set so that the overflow water depth was the same as in the experiment, and h was set to 0.5 m. The particle diameter of the sand used was the parameter d (= 0.394 mm), which is the closest particle diameter to the sand used in the experiment. Details are shown in Table 2. Various ground parameters are shown in Table 3.

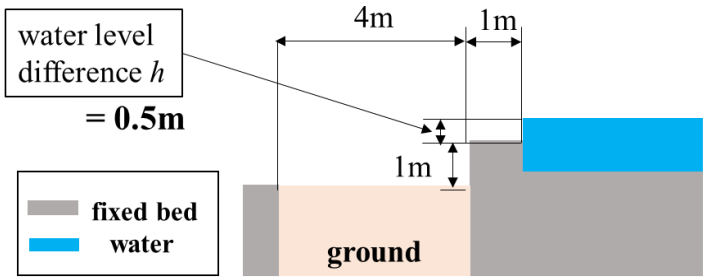


**Figure 4. Modeling in the numerical calculation.**

| | | |
|---|---|---|
| Grid size | x[m] | 0.025 |
| | y[m] | 0.025 |
| | z[m] | 0.025 |
| Time increment $\Delta t$ | | 1.0E-4 |
| Difference scheme | VP-DONOR | 1.0 |
| Flow velocity / pressure boundary conditions | | FREE |
| Boundary condition of VOF function F | | FREE |

**Table 2. Calculation conditions.**

| Various parameters of ground | | |
|---|---|---|
| Particle size[mm] | $d_S$ | 0.394 |
| Bed load coefficient | const a | 2.6 |
| Hoisting factor | const b | 1.60E-05 |
| Settling velocity[m/s] | $w_0$ | 0.050116 |
| Critical friction coefficient[m/s] | $u_C$ | 0.016634 |
| Maximum concentration of suspended sand layer | $C_{S\_max}$ | 1 |
| Saturated suspended sand concentration | $C_S$ | Automatic setting according to flow rate |
| Watanabe equation coefficients | $\varepsilon$ | 2 |

**Table 3. Various parameters of ground.**

**Results**

Figure 5 shows the flow field in the calculation. Figure 6 shows the comparison of experimental result and calculation result about the form of the sandy ground. The maximum scouring depth and its location, which are the two most important parameters for discussing scouring, coincide. The maximum scour depth is about 1 m, which occurs about 1.5 m from the upright seawall.

Figure 7 compares the time-series changes of the maximum scour depth. In the numerical calculation, after about 11 seconds, the sandy ground is almost in a steady state, and no scouring is promoted. However, in the previous experiment by Arikawa et al. (2014), the steady state of the sandy ground occurred after 200 seconds. The calculation result is about 20 times faster than the experimental value.

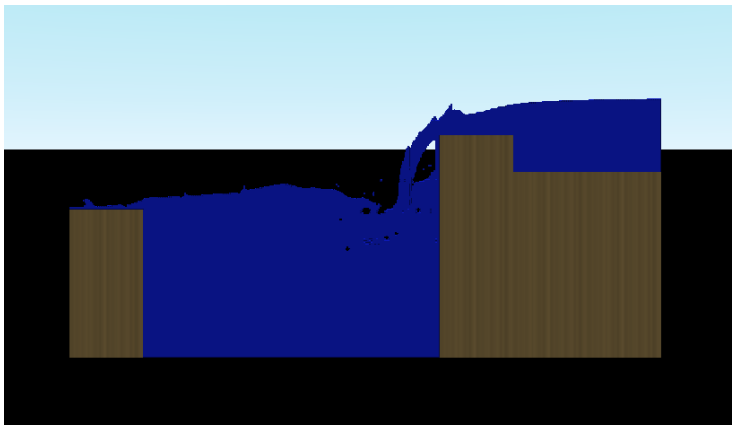

**Figure 5. Flow field in calculation.**

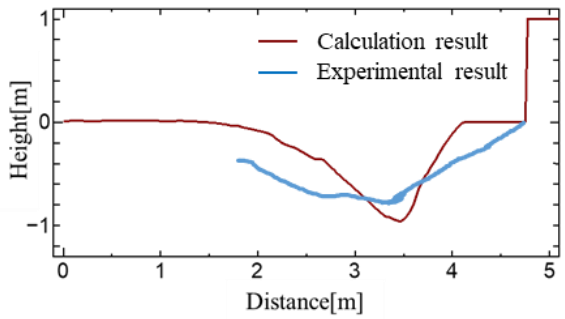


**Figure 6. Comparison of experimental result and calculation result**

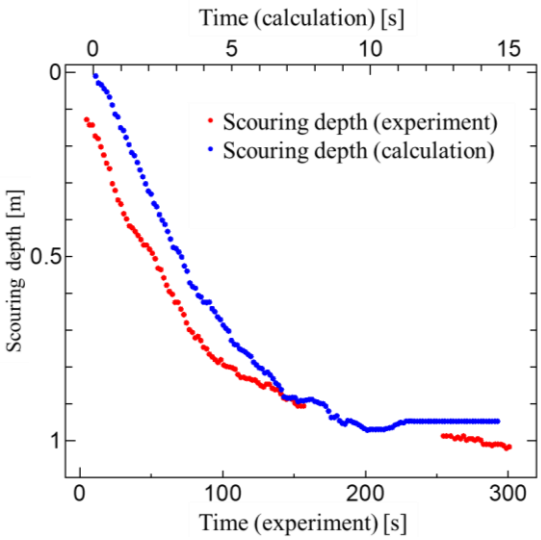


**Figure 7. Time series changes of the maximum scour depth.**

**Examination of the scour speed**

To increase the parameters that affect scour rate, the second and third terms of Equation (12) are conceivable. The topographic change caused by friction velocity has the greatest influence on the scour depth.

Among the terms to be increased, we attempted to change the bottom slope $\varepsilon$ to 10.0, to examine its effect on scour speed. The results are shown in Figure 8 and Figure 9. No scouring occurs when $\varepsilon$ is 0.0 and 0.1. Comparing the case $\varepsilon = 2.0$ and $\varepsilon = 10.0$, the larger the values, the more the scouring seems to extend in the horizontal direction. The scour speed is almost the same.

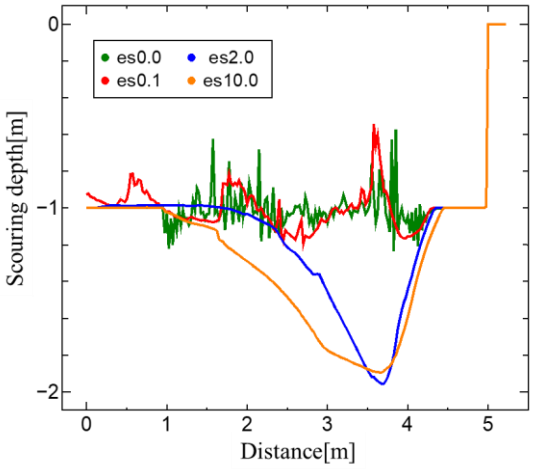


**Figure 8. Results from changing $\varepsilon$.**

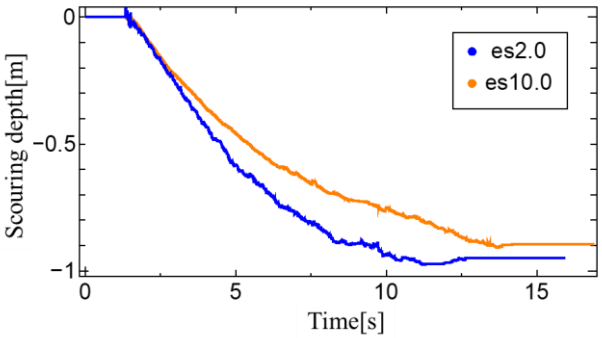


**Figure 9. Time series changes from changing $\varepsilon$.**

In addition, we tried increasing the upper limit of the concentration in the suspended sand layer until $C_{S\_max} = 0.337$ and $C_{S\_max} = 1.0$. The results are shown in Figure 10 and Figure 11. There was also no change in scour rate even when the concentration was adjusted.

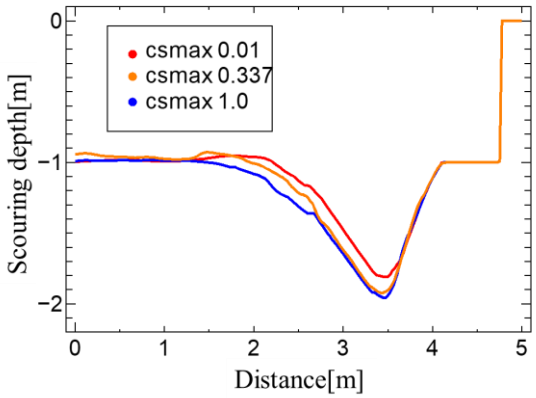


**Figure 10. Results for changing $C_{S\,max}$.**

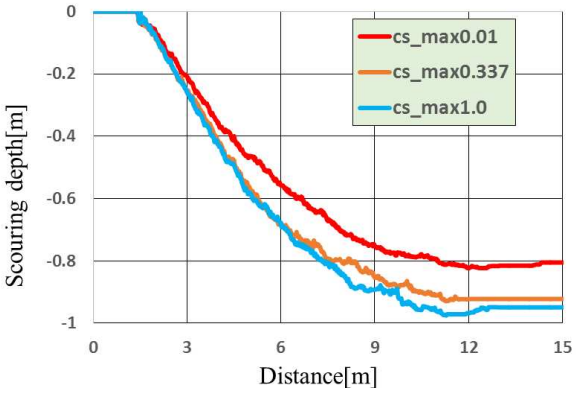


**Figure 11. Time series changes for changing $C_{S\,max}$.**

## CONCLUSIONS

- The scour depth and scour location were almost the same as the experimental values; however, the scour rate was about 20 times faster than in the experiment.
- The results of examining the coefficient of the bottom slope ε, showed that scouring was not reproduced when ε was 0.0 and 0.1. In addition, when ε was compared with 2.0 and 10.0, the scouring extended in the horizontal direction when $\varepsilon = 10.0$.
- The maximum suspended sand concentration was set at 1.0, 0.377, and 0.01, but the scour speed did not change.

As a future task, it is necessary to identify various parameters that affect the scour rate. In addition, the sand volume coefficient and the lifted sand volume coefficient will be examined, and the effect of the grid size on scour depth will be examined.

## REFERENCES


Taro ARIKAWA (2014), "*Experimental Study on Scour behind Seawall due to Tsunami Overflow",* Journal of Japan Society of Civil Engineers, Vol.70, No.2, I_926-I_930.

Tomoyuki TAKAHASH I(1999) , "*Development of a Tsunami Moving Bed Model Considering Exchanged Sediment Volume between Bed Load Layer and Suspended Sand Layer",* Journal of Japan Society of Civil Engineers, Vol.46, No.2, 606-610.

Takuzo SHIMIZU (1983), "*Beach Deformation and Drift Amount Model in Wave and Beach Flow Coexisting Field",* Journal of Japan Society of Civil Engineers, Vol.30.

Akira WATANABE (1984), "*Numerical Model of Three-Dimensional Beach Deformation due to Installation of Structures",* Journal of Japan Society of Civil Engineers, Vol.31.

Kohei SUZUKI (2019), "*Examination of Time Series Change of Scour Behind Seawall due to Overflow",* Journal of Japan Society of Civil Engineers, Vol.75, No.2, I_715-I_720.